Check for updates

# A new formation strategy of hybrid perovskites via room temperature reactive polyiodide melts†

Andrey A. Petrov, [ID] [a] Nikolai A. Belich, [a] Aleksei Y. Grishko, [a] Nikita M. Stepanov, [a] Sergey G. Dorofeev, [b] Eugene G. Maksimov, [c] Andrei V. Shevelkov, [b] Shaik M. Zakeeruddin, [d] Michael Graetzel,*[d] Alexey B. Tarasov [ID] *[ab] and Eugene A. Goodilin[ab]

Here we introduce a new solvent-free preparation method for hybrid metal halide perovskites involving the direct reaction of metallic lead with polyiodide melts. We discovered new reactive polyiodide melts (RPMs) that can be prepared simply by adding elemental iodine to halide salts of the organic A cations of common hybrid perovskites, *e.g.* methylammonium iodide (MAI) and formamidinium iodide (FAI), and their corresponding bromide salts MABr and FABr. For MAI/$I_2$ ratios ranging from 1:1 to 1:3 they form room temperature ionic liquids containing polyiodide anions and organic counterions. We find that metallic lead can be converted within a few seconds into pure or mixed cation/anion large-grain perovskite films of high electronic quality by a reaction with the RPM. The melts can dissolve also lead derivatives, opening up a realm of opportunities for future development of self-flux growth, liquid phase epitaxy and crystallization of perovskites for solar cell applications.

## Conceptual insights

The potential of existing methods for hybrid perovskite synthesis is almost fully explored at the moment; thus the community is enthusiastic about exploring new techniques to form perovskite layers and reveal their capability. Herein we demonstrate a novel strategy which includes reaction of metallic lead with new precursors – reactive polyiodide melts (RPMs). RPMs can be easily prepared by mixing $I_2$ with MAI (FAI), resulting in highly-viscous liquids at room temperature. This unique composition acts simultaneously as a liquid medium and precursor, thus providing sufficient supply of precursors and exhibiting high reactivity. These properties of the newfound compounds allow obtaining perovskite films consisting of micrometer-scale crystals and exhibiting intense photoluminescence. The proposed strategy show promising potential and may pave a new way towards efficient solar cells.

## Introduction

Hybrid organic–inorganic halide perovskites with the general formula $APbX_3$ (A = $CH_3NH_3^+$, $CH(NH_2)_2^+$; X = Cl, Br, I) are considered to be highly promising materials for next-generation solar cells owing to their strong light absorption,[1] large electron and hole diffusion lengths,[2] and low cost and facile fabrication using solution-processing methods.[3,4] The power conversion efficiency of hybrid perovskite solar cells demonstrated an outstanding growth from ∼4% in 2009 to more than 22% in 2016,[5]

making the perovskites one of the most attractive classes of light harvesting materials for future photovoltaics.[6]

To achieve a high solar to electric power conversion efficiency (PCE), the absorbing layer of solar cells has to satisfy strict requirements for the morphology of the perovskite layer such as a large lateral size of perovskite crystallites, excellent crystallinity, and high uniformity of the perovskite films.[7] The most efficient solar cells are produced by one- or two-step solution-based methods. The former provides crystallization of the perovskite from solvents like dimethylformamide (DMF), dimethylsulfoxide (DMSO), γ-butyrolactone (GBL) or their mixtures, whereas the two-step approach includes deposition of a lead precursor (typically $PbI_2$) followed by its conversion into the perovskite. The solution deposition approach was further developed by means of heating of substrates,[8] using additives,[9] performing post-heat-treatment[10] and solvent annealing.[11] Deposition of a perovskite layer by using polar aprotic solvents necessarily involves the formation of intermediate adducts that severely complicates control over crystal morphology.[12–15]

Other strategies include vapor deposition of the components either simultaneously or sequentially. The films thus obtained exhibit high uniformity and crystallinity; however, this group of methods significantly complicates the deposition process,

[a] *Laboratory of New Materials for Solar Energetics, Department of Materials Science, Lomonosov Moscow State University, Lenin Hills, 119991, Moscow, Russia. E-mail: alexey.bor.tarasov@gmail.com*

[b] *Department of Chemistry, Lomonosov Moscow State University, Moscow, Lenin Hills, 119991, Moscow, Russia*

[c] *Department of Biology, Lomonosov Moscow State University, Moscow, Lenin Hills, 119991, Moscow, Russia*

[d] *Laboratory of Photonics and Interfaces Institute of Chemical Sciences and Engineering École Polytechnique Fédérale de Lausanne (EPFL), Station 6, CH-1015 Lausanne, Switzerland. E-mail: michael.graetzel@epfl.ch*

† Electronic supplementary information (ESI) available. See DOI: 10.1039/c7mh00201g

requires sophisticated equipment, and gives no superior efficiencies compared to the solution-based approach.[7,16]

As the potential of these methods is by now fully explored and these methods provide at this stage only incremental improvements, new techniques to form perovskite layers with more flexible control over the morphology are warranted. As soon as perovskite solar cells demonstrate real promise to enter the market, it is also important that such new methods should be applicable to form perovskite layers on a large scale.

While being widely used in semiconductor production, a large group of well-developed methods of crystal growth from melts or fluxes is still inapplicable in perovskite photovoltaics, as the key components, MAI and $PbI_2$, are unable to form a melt at moderate temperatures below perovskite decomposition thresholds: MAI forms a pre-melting state called an ionic plastic phase at 148 °C, $PbI_2$ melts at 402 °C and there are no eutectics found in this binary system. At the same time, the perovskite itself decomposes into MAI and $PbI_2$ already at ~150 °C.[17–19]

Here, we describe a novel and highly versatile strategy for hybrid perovskite film growth for solar cells using new room temperature melts of methylammonium and formamidinium polyiodides with the general formulae "$MAI_{3+x}$" and "$FAI_{3+x}$".

## Results and discussion

The new polyiodide melts can be easily obtained by simple mixing MAI (and/or FAI) powders with crystalline iodine (Fig. 1). The process starts instantly and proceeds rapidly, resulting in the formation of highly-viscous liquids with a metallic shine (Fig. 1). RPMs are dark brown in transmission light (see absorption spectra in Fig. S1, ESI†). "$MAI_{3+x}$" and "$FAI_{3+x}$" polyiodide melts exhibit freezing points below 20 °C, being liquid at room temperature and above. Thus they provide analogues to the well-known classical production technologies of traditional semiconductors from melts.

Some other polyiodides with organic cations, i.e. $MeEt_3NI_9$, $MeEt_3NI_{11}$, $Oc_4NI_5$, $Oc_4NI_7$, $Oc_4NI_9$, and $Oc_4NI_{11}$, where Oc stands for n-octyl, have been reported to form ionic liquids at room temperature[20–22] and a liquid-crystalline state in the case of 1-methyl-3-propylimidazolium polyiodide.[22] Although cesium, ammonium and tetraalkylammonium polyiodides possessing similar structures had been described as early as at the end of the 19th century and the first quarter of the 20th century,[23–26]

methylammonium and formamidinium polyiodide melts have not been reported so far.

We found that polyiodide melts can easily and quickly react with metallic lead and some lead compounds, such as $PbI_2$ and PbO, to form perovskites (Fig. S5, ESI†). This seems to be a brilliant example of a direct binary synthesis without side products since "$MAI_3$" and "$FAI_3$" contain all necessary components in an equimolar ratio, except for the lead, to form $MAPbI_3$ and $FAPbI_3$, respectively. In this case, the interaction of a metallic lead readily leads at once to the formation of the perovskite phase following the amazing cross-reaction: $MAI_3$ (liquid) + Pb (solid) → $MAPbI_3$ (solid). Such a conversion proceeds at room temperature (or upon mild heating for some compositions of $MAI_{3+x}$ and $FAI_{3+x}$) and results in highly crystalline continuous films consisting of large crystallites that exhibit intense photoluminescence and long lifetimes of charge carriers. It should be underlined that the MAI and FAI-based polyiodide melts act both as a solvent and as a reagent, providing oxidation of metallic lead followed by the formation of perovskite crystals within a few seconds. Thus, we suggest a new term, reactive polyiodide melts (RPMs), to denote their unique function in the process of perovskite formation.

We studied the local structure of the RPM by Raman scattering spectroscopy (RSS) using different laser excitation wavelengths to probe resonant and regular excitation modes (Fig. 2 and Fig. S2 in the ESI†). All spectral characteristics indicate that the liquid layers formed by multi-component melts ($MAI/MABr/FAI–I_2$) exhibit several intense vibrational modes (Fig. 2, also Fig. S2 in the ESI†) being different from solid iodine which is characterized usually by a set of bands at 180, 190, 214, 368 and 425 $cm^{-1}$.[20,21] The highest energy peak of RPMs at 95–110 $cm^{-1}$ is characteristic of the room temperature polyiodide melts and corresponds surely[20,21,27] to the symmetric stretch of triiodide ions. Its position is shifted by more than 70 $cm^{-1}$ compared to the molecular iodine band at 180 $cm^{-1}$ due to its peculiar electronic structure, namely, delocalized σ-bonding that is missing in $I_2$.[27] The next resolved intense peak at about 160–170 $cm^{-1}$ is shifted to higher energies by about 10–20 $cm^{-1}$ with respect to the 180 $cm^{-1}$ band of pristine $I_2$. We attribute it to adducts like $I_3^-\cdot(I_2)_n$ with a variable strength of I–I bonds which causes the shift in Raman spectra due to iodine molecules surrounding the triiodide ions. They do not necessarily correspond to true high order polyiodides with their own electronic structure; instead, triiodide ions seem to exist separately and perturb the surrounding $I_2$ preserving
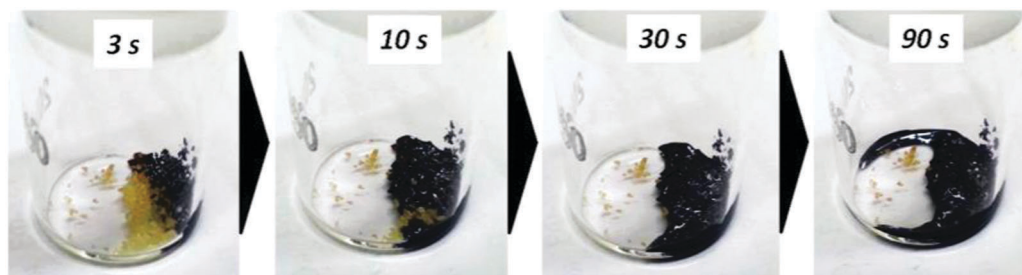


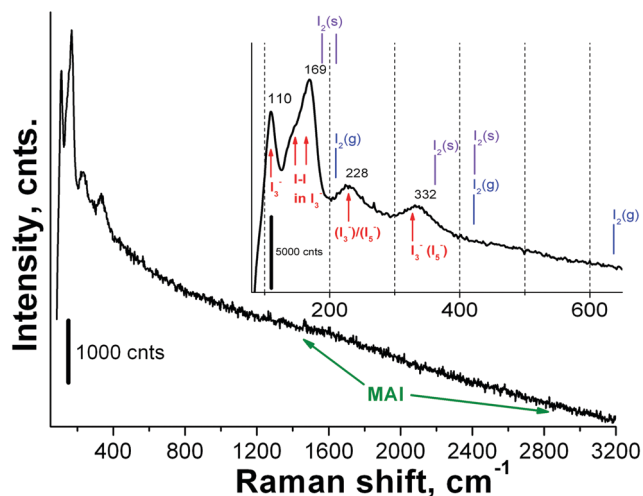Fig. 1 The formation dynamics of a liquid polyiodide $MAI_x$ by mixing MAI and iodine powders.

**Fig. 2** A typical resonant Raman spectrum of an RPM of the MAI/$I_2$ = 0.9 : 1 composition within an extended spectral range. The inset shows strong modes of the $I_3^-$ ion (110, 169 cm$^{-1}$) with a possible contribution of longer polyiodides/$I_3^-$ overtones at 228 and 332 cm$^{-1}$. No peak of free iodine is observed. MAI vibrations are not visible because of the high intensity of the background of polyiodides resonantly irradiated with a green 514 nm laser (1.5 mW output power, 10 s acquisition time, illuminated area 100 μm$^2$).

different bonding in $I_3^-$ and $I_2$ of the adducts $I_3^- \cdot (I_2)_n$. In these terms, this iodine is different from pure solid or gaseous $I_2$ and might be called iodine "solvating" the $I_3^-$ and forming an extended network of $I_3^-$ and $I_2$ chains resulting in an experimentally observed increased viscosity of RPMs. Examples of such adducts can be found in the literature.[27] Also, no typical iodine peaks could be observed in the molten samples since the two minor peaks at about 220–230 and 330–340 cm$^{-1}$ are either overtones of triiodides or more complex polyiodides.[20,21,27] These peaks exist under conditions of resonant laser irradiation (633 and 514 nm) and disappear completely if an IR laser is used for Raman excitation; thus they should not be attributed to molecular iodine (see Fig. S2, ESI†).

It should also be noted that the polyiodides absorb emission at 514 and 633 nm resonantly, and this drastically increases the intensities of their vibration modes, preventing observation of MA$^+$/FA$^+$ vibrations that appear only if an IR laser is used

(see Fig. S2, ESI†). In this context, FAI/$I_2$ and MAI/$I_2$ liquids give very similar spectra. Interestingly, the ratio between the intensities of the two mentioned most intense high energy Raman modes for triiodides and solvating iodine correlates very well with the MAI/$I_2$ ratio in the melts (see the ESI†); the excess of MAI/FAI stabilizes obviously triiodides, making the $I_3^-$ stretching mode the most intense one, while the iodine-rich RPM shows a brighter peak of solvating iodine. This allows monitoring the melt composition even in polyphase mixtures, confirming that the liquid phase range covers approximately the compositions varying between MAI/$I_2$ = 1 : 1–1 : 3.

Dissolution of lead or replacing partly MA$^+$ with FA$^+$ in the melt does not change the spectra drastically; therefore, their local structure remains almost the same as observed for pure MAI–$I_2$ liquids. MA and FA cations are expected to form hydrogen bonds with polyiodide, decreasing the charge density of the polyiodide, which should affect the position of the Raman bands. However, this effect was not observed which might be connected with the strong "solvation" of $I_3^-$ with iodine, thus shielding the interaction of MA/FA with polyiodides. The oxidation of Pb by $I_3^-$ would form Pb$^{2+}$ and I$^-$ ions in the melt, which in turn would generate PbI$_2$ or PbI$_3^-$. We cannot determine the exact nature of the lead species in the melt since the content of lead in RPMs is only a few atomic percent according to our experimental estimations.

A perovskite layer on a glass substrate was obtained by the above-mentioned reaction of the RPM (MAI/$I_2$ = 1 : 2) deposited by spin-coating onto 100–500 nm thick metallic lead films (see the Experimental section for details). It takes approximately 30 s for the RPM to convert the 250 nm thick film of Pb completely as judged by the disappearance of the Pb metal reflection that can be monitored from the back side of the glass substrate. In the case of thicker films, the growth of perovskite retards the lead conversion, and therefore, a reflecting surface of metallic lead residues may be observed after spin-coating of RPMs. We used two ways of removal of the excess of the RPM that yielded slightly different morphologies. In the first approach, unreacted polyiodide was removed by annealing at 115 °C for 10 minutes, leaving behind some excess MAI partially converted into perovskite. This results in round-shaped crystals of perovskite in some areas (Fig. 3a). The XRD analysis (Fig. S3, ESI†) showed that the
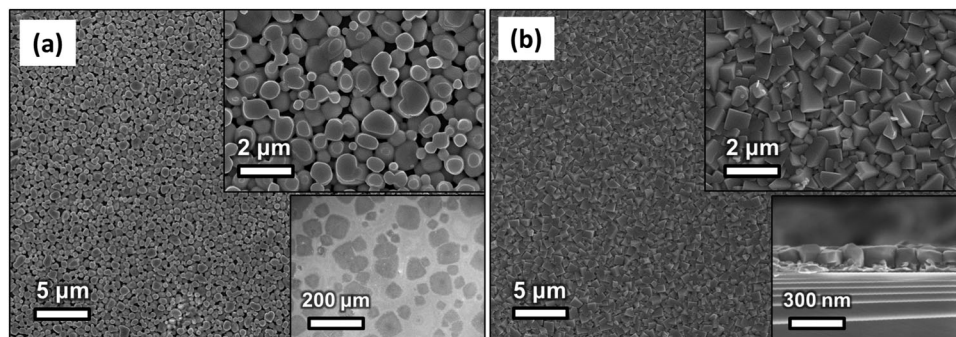


**Fig. 3** Top view SEM images for the two types of perovskite morphologies obtained by annealing (a) and rinsing in isopropanol (b) of the freshly spin-coated film (the right-bottom inset in (b) shows a cross-sectional SEM with large crystals across the film).

obtained film contained mostly the target MAPbI$_3$ phase and, also, unreacted Pb and a small amount of MAI as a component of the RPM.

In the second approach, the unreacted polyiodide was removed either by immediately rinsing with isopropanol or by gradually adding 1 mL of isopropanol for 5 seconds prior to the end of spinning. Highly uniform films with cubic crystals of MAPbI$_3$ up to 1 μm in size were thus obtained (Fig. 3b). According to the XRD data (Fig. 5b), the film contained MAPbI$_3$ perovskite and small traces of PbI$_2$. As evident from the morphological features, the perovskite film consists of interconnected cubes which results in complete surface coverage (Fig. S7, ESI†). This morphology is opposed to the one that is commonly observed when a film of a lead precursor is stored in a solution of MAI in i-PrOH, resulting in large cubes with large pinholes in between them.[28,29] We believe that the highly dense coverage stems from the following features of the perovskite film formation mechanism: (i) very high concentrations of MAI and I$_2$ in the melt instantly produce a large amount of nucleation centers across the whole area of metallic lead when the RPM is placed on top of the lead film; and (ii) extremely high reactivity and high diffusivity rates in the RPM enable intensive mass-transfer of the lead-precursor, providing fast growth of cubic grains and leading to the intergrowth of neighboring cubes.

Our new procedure is advantageous over solvent-based methods because it allows carrying out the reaction with high concentrations of reactants and requires no solvents, which is beneficial for industrial processing of perovskite solar cells. Another advantage of our method is the use of lead as an initial reactant since this metal as well as other lead precursors can be deposited by a highly efficient way using a large number of common deposition techniques, such as sputtering, electrodeposition, *etc.*, on different substrates, including flexible wafers. Importantly, the molar volume increases 8.4 times during the conversion of lead into perovskite, thus ensuring the formation of pinhole free films.

The MAI$_{3+x}$ and FAI$_{3+x}$ polyiodides exhibit very high reactivity with respect to lead and PbI$_2$. For instance, a 50 nm thick layer of Pb completely dissolves in MAI$_{3+x}$ polyiodide melts within several seconds (Fig. S4, ESI†). Even a 260 nm thick Pb film can be readily and quantitatively converted into a perovskite film. This striking observation can be rationalized in terms of two sequential steps: the oxidation of metallic lead to Pb(II) by iodine contained in the RPM followed by the dissolution of Pb into the MAI$_{3+x}$ and FAI$_{3+x}$ polyiodides under the formation of perovskite. When the saturation level of lead in the RPM is reached, the perovskite film grows further.

In order to investigate the reaction ability of lead with RPMs of different compositions and long-term phase formation in the ternary system MAI–Pb–I$_2$, we prepared four RPMs with MAI/I$_2$ ratios equal to 1:1, 1:2, 1:3, and 1:4. All the melts were homogeneous liquids at ambient or slightly increased temperature (40 °C). We added 20 mol% of metallic lead powder to the RPMs followed by vigorous stirring with a magnetic bar in sealed vials for 7 days. Finally, the solid part was separated from liquid by centrifugation and both fractions, liquid and solid, were analyzed by RSS and XRD respectively (Fig. 4).

Metallic lead does not coexist with the RPM – it reacts to form PbI$_2$, perovskite MAPbI$_3$, or their mixture depending on the initial composition of the reaction mixture. When the RPM is enriched with I$_2$ (1:4), the obtained product consists of PbI$_2$. The increase of MAI content in the RPM results in the increase of the MAPbI$_3$ fraction in the MAPbI$_3$/PbI$_2$ mixture. When the (1:2) RPM is used, the solid produced consists of perovskite with a small admixture of PbI$_2$. In the MAI–rich region (1:1) some new unidentified phase is formed that we expect to be 2D layered perovskites that were previously reported.[19]

The data on the reaction ability of RPMs and lead give also a clue on possible formation schemes of perovskites. For example, iodine evaporation at room temperature for the #1 sample gives expectedly MAI-rich needles, while the same process for the #4 sample results in almost pure ∼100–150 μm perovskite cubes (Fig. S6, ESI†) after isothermal liberation of iodine as a volatile component since the #4 compositional point belongs to the I$_2$–MAPbI$_3$ line. This fact therefore proves the concept of obtaining single-phase perovskites using such a simple approach.

The suggested application of RPMs opens up the possibility of obtaining other perovskite compounds. Using RPMs with mixed compositions prepared from MAI, FAI, MABr and I$_2$ we obtained films of δ-FAPbI$_3$, MA-stabilized FAPbI$_3$, MA$_x$FA$_{1-x}$PbI$_{3-y}$Br$_y$ perovskites and anion mixed MAPbI$_{3-x}$Br$_x$ as shown in Fig. 5 and Table S1 in the ESI.† The obtained films exhibit a uniform morphology with large crystals of about 1 μm in size (Fig. 5a). Single XRD peaks in the 13–19° range in the inset of Fig. 5b indicate that the obtained perovskite is a single phase rather than a mixture of phases. The position of the peaks is shifted relatively to the reference peak positions of the pure phase, which indicates the formation of mixed phases. Similarly to the MAPbI$_3$ film, XRD showed in some cases a small amount of PbI$_2$ in the samples, which we attribute to the small hexagonal crystals on the surface. The formation of secondary phases could be avoided by keeping the appropriate ratio of lead to the RPM in the reaction mixture (Fig. 4).

While the preparation of state of the art perovskite solar cells needs further optimization of the deposition process, we characterize here the electronic quality of the films in terms of charge carrier lifetime measured by time-resolved photoluminescence spectroscopy. The samples of both types of morphology exhibit maximum photoluminescence at 765–770 nm (Fig. 6), whereas the average lifetimes of charge carriers in the cubic morphology are one order of magnitude greater than those in the sphere-like morphology, with ∼71% of the charge carriers exhibiting a lifetime of 210 ns. This value is comparable to that reported for perovskite films in high-efficiency solar cells.[30] The slow components of the photoluminescence decay reflect the kinetics of first order trap controlled radiationless recombination of charge carriers according to the Shockley–Read mechanism. Longer lifetimes are expected to provide longer diffusion lengths,[10,31] thus allowing efficient minority charge collection. Time-resolved photoluminescence data on the films of mixed perovskites dipped in the IPA after spin-coating are presented in Table S1 of the ESI.†

A number of reports on the electronic trapping-states in lead-halide perovskite materials show that defects are localized
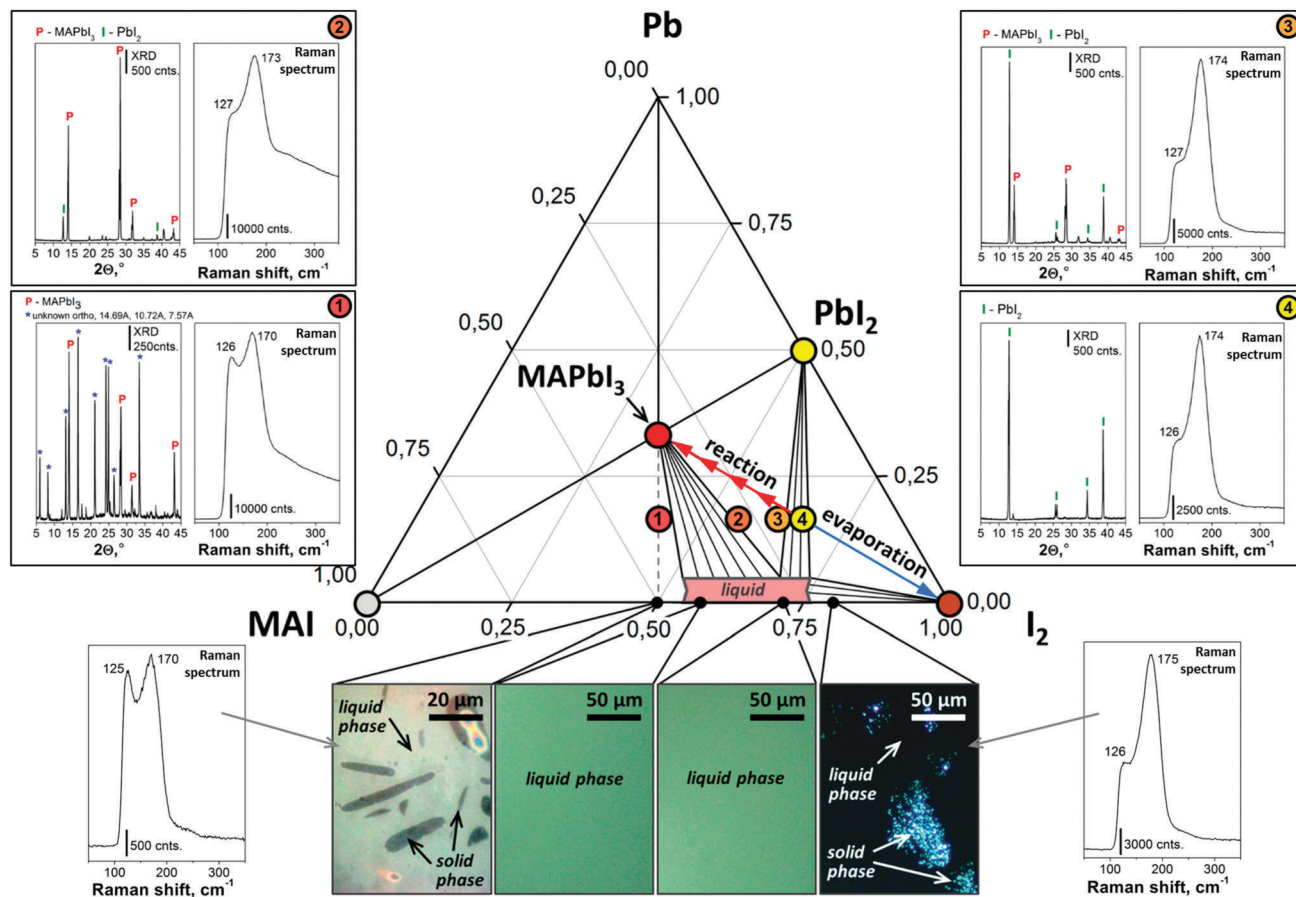
Fig. 4 Reactivity of metallic lead with RPMs together with reconstructed phase assemblage for one week interaction depicted on the Gibbs triangle. Closed circles "1"–"4" denote experimental compositions (#1–#4 samples), "P" denotes the perovskite (MAPI₃) phase, and the light-red field represents tentatively RPM liquid compositions available at room temperature. Tentative triangulations and phase fields are given according to separate XRD and RSS analyses of solid and liquid fractions of the products of lead interaction with RPMs of different compositions as shown in double plots of XRD/RSS patterns of the #1–#4 samples around the triangle. The bottom optical pictures and RSS plots correspond to pure MAI/I₂ precursor RPMs of 1:1–1:4 component ratios without lead. The arrows within the RPM visible layer indicate solid phases of iodine crystals for the 1:4 RPM and, also, unknown orthorhombic phase crystals with $a$ = 14.69 Å, $b$ = 10.72 Å, and $c$ = 7.57 Å marked with blue asterisks in the XRD pattern of the #1 sample.
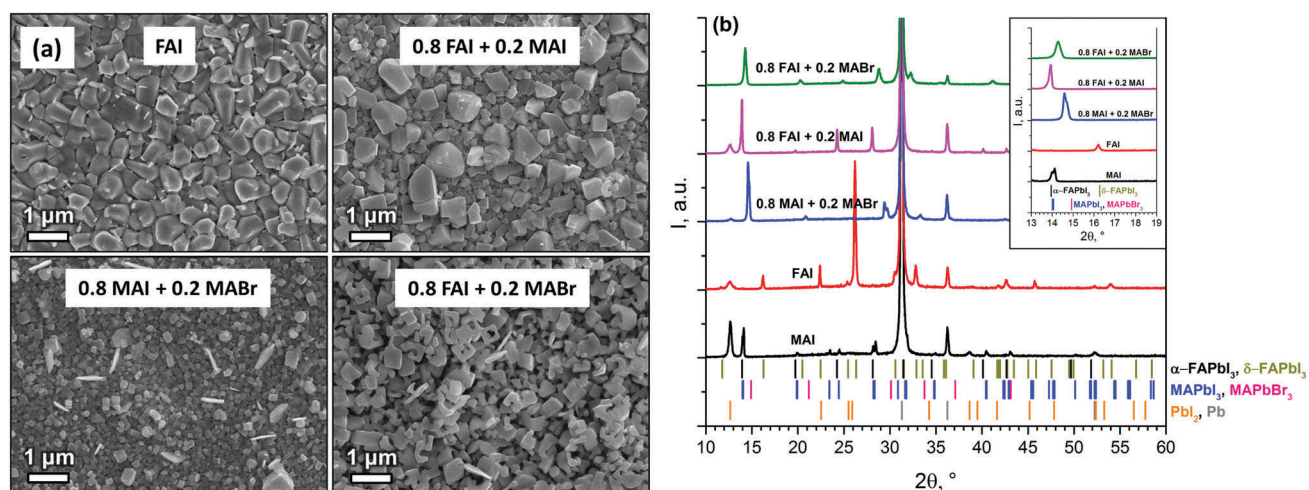


Fig. 5 (a) SEM images of the films obtained from the mixed RPM (dipped in the IPA after spin-coating) and (b) XRD spectra of the films obtained from various polyhalides.
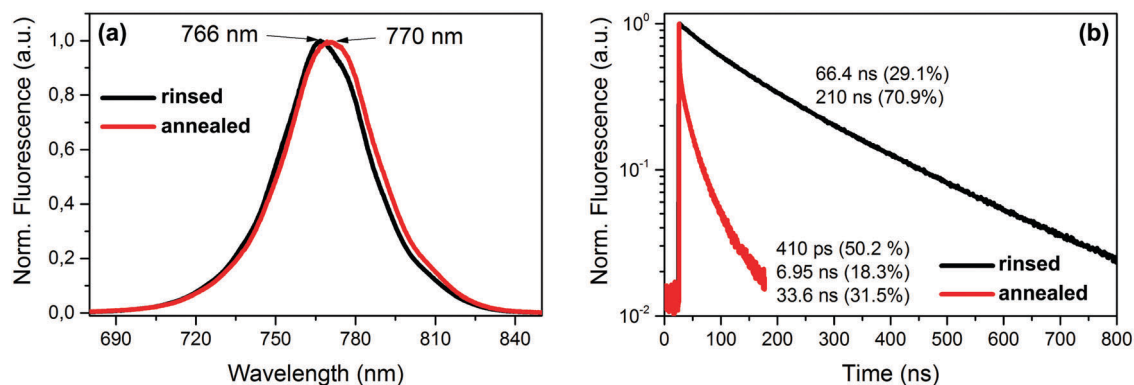
Fig. 6 Effect of the perovskite morphology on (a) the emission spectra and (b) the photoluminescence decay kinetics with estimated lifetimes of charge carriers.

predominately on the surface of the crystals.[32] Hence the observed long luminescence lifetimes are likely to originate from a low trap-density that in turn arises from the high volume-to-surface ratio of the perovskite films that are comprised of strongly interconnected cubes of perovskites. Although the measured value of 210 ns is shorter than the microsecond carrier lifetimes observed in very large crystals[2] of perovskite, our RPM preparation strategy provides good perspectives to generate high electronic quality perovskite films.

## Conclusions

We discovered a new class of ionic liquids of the generic formula $MAX_{(3+y)}$ or $FAX_{(3+y)}$, where X stands for halide and $y(>0)$ is a stoichiometric coefficient. We show that these ionic liquids that can serve as reagents to produce metal halide perovskites form metallic lead in a simple one step conversion process. We prepared the liquid reagents for solar cell perovskite fabrication *i.e.* methylammonium and formamidinium polyiodides (reactive polyiodide melts, RPMs) – by simply mixing MAI (FAI) and elemental iodine. Our new solvent-free route for the synthesis of hybrid organic–inorganic perovskites proceeds rapidly upon spreading the RPMs over metallic lead films. This results from the high reactivity of RPMs, providing a simple and scalable means of perovskite film preparation through the robust, effective, and technologically advantageous process. It requires no solvent for deposition and can be conducted at room temperature. Moreover, we showed proof of concept of perovskite crystallization directly from the melt with dissolved lead. This new strategy will, for the first time, open access to classical methods of crystal growth from melts, such as liquid-phase epitaxy, which is well known for semiconductors.

## Methods and materials

### Liquid polyiodide preparation

Liquid polyiodides were obtained from iodine (99% purity, Ruskhim), MAI, MABr, and FAI (99.9% purity, Dyesol). The MAI, MABr, FAI and $I_2$ were ground in a mortar for several minutes and

Table 1 Compositions of the samples #1–#4 mapped on the diagram $MAI–I_2–Pb$ (Fig. 4)

| Sample | MAI, mg (mmol) | $I_2$, mg (mmol) | Pb, mg (mmol) |
|---|---|---|---|
| #1 | 181.8 (1.1435) | 290.5 (1.1435) | 94.7 (0.4574) |
| #2 | 121.2 (0.7623) | 387.3 (1.5247) | 94.7 (0.4574) |
| #3 | 90.9 (0.5718) | 435.7 (1.7153) | 94.7 (0.4574) |
| #4 | 72.7 (0.4574) | 464.7 (1.8296) | 94.7 (0.4574) |

mixed in different proportions in a weighing bottle. The compounds reacted instantly, forming a brown liquid. After shaking the mixtures for 30 minutes, homogeneous liquids were obtained. Detailed compositions used are listed in Table S1, ESI.†

Mixtures for the study of the long term reaction of lead with polyiodides were prepared by adding 20 mol% of metallic lead powder to the preliminarily prepared polyiodide melts followed by their reaction in sealed vials with magnetic stirring for one week. The detailed compositions are given in Table 1.

### Perovskite film preparation

Perovskite films were obtained in an ambient atmosphere by treating metallic lead films with polyiodides or their mixtures. Thin films of lead with a thickness of 50 to 240 nm were deposited on glass substrates by vacuum thermal evaporation in the deposition system VUP-5 in a vacuum of $10^{-5}$ Torr. A portion of the lead vaporized from a Mo boat section of $15 \times 0.2$ mm$^2$ by heating under an electric current of 100 A. The shortest distance from the evaporator to the substrate is 185 mm. The average film growth rate was $\sim 300$ nm s$^{-1}$. An excess of liquid polyiodide (20 μL) was spin-coated onto the lead film for 30 seconds at 3000 rpm. Unreacted polyiodide was eliminated through one of three ways: casting 100 μL of isopropanol onto the spinning film, washing the film in a baker filled with isopropanol or annealing the film at 115 °C for 15 minutes.

### Characterization

The materials were characterized by scanning electron microscopy (SEM) using Zeiss Supra 40. XRD patterns were examined using a Rigaku D/MAX 2500 (Japan) with a rotating copper anode (CuK$_\alpha$ irradiation, 5–80° $2\theta$ range, 0.02° step). Diffraction maxima

were indexed using the PDF-2 database. UV-vis absorption spectra were recorded using the UV-vis spectrophotometer Lambda 950 (Perkin-Elmer) with an attached diffuse reflectance accessory.

The photoluminescence decay kinetics of the samples were measured *via* a home-built inverted microscope with a spatial resolution of up to 50 μm and time resolution of up to picoseconds. A microscope was connected to a time- and wavelength-correlated single photon counting setup based on an SPC-150 module and an HMP-100-50 detector (Becker&Hickl, Germany). Samples were photoexcited using a 450 nm laser diode (InTop, Russia) delivering 30 ps (FWHM) pulses, driven at repetition rates from 100 kHz up to 50 MHz or in CW mode. The necessary spectral band was selected by using a ML44 monochromator (Solar, Belarus). For the steady-state measurements of fluorescence the spectral detector was replaced with an USB4000 + CCD spectrometer (Ocean Optics, USA). Time-courses of the fluorescence intensity at a single wavelength were recorded using the strip-chart mode in SpectraSuite software (Ocean Optics, USA). Fluorescence decay curves were approximated by a sum of exponential decay functions with the SPC Image (Becker and Hickl, Germany) software package. To compare different decay curves, we calculated the average decay time according to the following expression $\tau_{av} = \sum_{i}^{n} \tau_i a_i$, where $\tau_i$ and $a_i$ are the lifetime and the amplitude (normalized to unity: $\sum_{i}^{n} a_i = 1$) of the $i$-th fluorescence decay component, respectively. All experiments were performed at room temperature.

Raman experiments were performed using an InVia Raman microscope (Renishaw, UK) equipped with 514, 633 and 785 nm laser sources and power neutral density filters. All the spectra were collected using ×50 long focus objective, 1–100% laser power and 10–120 s of acquisition time. The laser power on the samples was about 1–15 mW per 2 micrometer spot size. A silicon wafer was used for preliminary calibration. To avoid evaporation of iodine and identify phases, the samples were squeezed between two thin pieces of glass and slightly mechanically joined together. An exact position of the 10–20 micron spot of the laser was controlled using an optical system.

The homogeneity of the polyiodide mixtures was inspected using a Metallographic optical microscope Eclipse 600 POL, and the samples were prepared by squashing 5 μL of liquids in a thin layer between two slides.

## Author contributions

A. A. P. wrote the manuscript in cooperation with A. B. T., E. A. G. and M. G. A. A. P., N. A. B., A. Y. G. and N. M. S. designed and conducted the experiments. S. G. D. carried out lead deposition. A. B. T., E. A. G., A. V. S., S. M. Z. and M. G. performed scientific evaluation of data. A. B. T. supervised the project. All of the authors discussed and analyzed the data.

## Acknowledgements

## References

1 Q. Lin, A. Armin, R. C. R. Nagiri, P. L. Burn and P. Meredith, *Nat. Photonics*, 2015, **9**, 106–112.

2 Q. Dong, Y. Fang, Y. Shao, P. Mulligan, J. Qiu, L. Cao and J. Huang, *Science*, 2015, **347**, 967–970.

3 P. Gao, M. Grätzel and M. K. Nazeeruddin, *Energy Environ. Sci.*, 2014, **7**, 2448.

4 Y. Zhao and K. Zhu, *Chem. Soc. Rev.*, 2016, **45**, 655–689.

5 National Renewable Energy Laboratory (NREL), http://www.nrel.gov/pv/assets/images/efficiency-chart.png, accessed May 12, 2017.

6 M. Saliba, T. Matsui, J.-Y. Seo, K. Domanski, J.-P. Correa-Baena, M. K. Nazeeruddin, S. M. Zakeeruddin, W. Tress, A. Abate, A. Hagfeldt and M. Grätzel, *Energy Environ. Sci.*, 2016, **9**, 1989–1997.

7 N.-G. Park, *Nano Convergence*, 2016, **3**, 15.

8 W. Nie, H. Tsai, R. Asadpour, J.-C. Blancon, A. J. Neukirch, G. Gupta, J. J. Crochet, M. Chhowalla, S. Tretiak, M. A. Alam, H.-L. Wang and A. D. Mohite, *Science*, 2015, **347**, 522–525.

9 Y. Chen, M. He, J. Peng, Y. Sun and Z. Liang, *Adv. Sci.*, 2016, **3**, 1500392.

10 F. X. Xie, D. Zhang, H. Su, X. Ren, K. S. Wong, M. Grätzel and W. C. H. Choy, *ACS Nano*, 2015, **9**, 639–646.

11 Z. Xiao, Q. Dong, C. Bi, Y. Shao, Y. Yuan and J. Huang, *Adv. Mater.*, 2014, **26**, 6503–6509.

12 Y. Guo, K. Shoyama, W. Sato, Y. Matsuo, K. Inoue, K. Harano, C. Liu, H. Tanaka and E. Nakamura, *J. Am. Chem. Soc.*, 2015, **137**, 15907–15914.

13 J. Cao, X. Jing, J. Yan, C. Hu, R. Chen, J. Yin, J. Li and N. Zheng, *J. Am. Chem. Soc.*, 2016, **138**, 9919–9926.

14 A. A. Petrov, N. Pellet, J.-Y. Seo, N. A. Belich, D. Y. Kovalev, A. V. Shevelkov, E. A. Goodilin, S. M. Zakeeruddin, A. B. Tarasov and M. Graetzel, *Chem. Mater.*, 2017, **29**, 587–594.

15 F. Hao, C. C. Stoumpos, Z. Liu, R. P. H. Chang and M. G. Kanatzidis, *J. Am. Chem. Soc.*, 2014, **136**, 16411–16419.

16 S. Brittman, G. W. P. Adhyaksa and E. C. Garnett, *MRS Commun.*, 2015, **5**, 7–26.

17 C. C. Stoumpos, C. D. Malliakas and M. G. Kanatzidis, *Inorg. Chem.*, 2013, **52**, 9019–9038.

18 B. Brunetti, C. Cavallo, A. Ciccioli, G. Gigli and A. Latini, *Sci. Rep.*, 2016, **6**, 31896.

19 Z. Song, S. C. Watthage, A. B. Phillips, B. L. Tompkins, R. J. Ellingson and M. J. Heben, *Chem. Mater.*, 2015, **27**, 4612–4619.

20 L. A. Bengtsson, H. Stegemann, B. Holmberg and H. Füllbier, *Mol. Phys.*, 1991, **73**, 283–296.

21 H. Stegemann, A. Rohde, A. Reiche, A. Schnittke and H. Füllbier, *Electrochim. Acta*, 1992, **37**, 379–383.

22 V. K. Thorsmølle, J. C. Brauer, S. M. Zakeeruddin, M. Grätzel and J. E. Moser, *J. Phys. Chem. C*, 2012, **116**, 7989–7992.

23 R. M. Bozorth and L. Pauling, *J. Am. Chem. Soc.*, 1925, **47**, 1561–1571.

24 F. D. Chattaway, *J. Chem. Soc., Trans.*, 1915, **107**, 105–108.

25 F. D. Chattaway and G. Hoyle, *J. Chem. Soc., Trans.*, 1923, **123**, 654–662.

26 G. S. Johnson, *J. Chem. Soc., Trans.*, 1878, **33**, 397–401.

27 P. H. Svensson and L. Kloo, *Chem. Rev.*, 2003, **103**, 1649–1684.

28 Y. He, Y. Lei, X. Yang, K. Lu, S. Liu, L. Gu and Z. Zheng, *Appl. Surf. Sci.*, 2016, **389**, 540–546.

29 J.-H. Im, I.-H. Jang, N. Pellet, M. Grätzel and N.-G. Park, *Nat. Nanotechnol.*, 2014, **9**, 927–932.

30 T. M. Brenner, D. A. Egger, L. Kronik, G. Hodes and D. Cahen, *Nat. Rev. Mater.*, 2016, **1**, 15007.

31 T. C. Sum and N. Mathews, *Energy Environ. Sci.*, 2014, **7**, 2518–2534.

32 T. Leijtens, G. E. Eperon, A. J. Barker, G. Grancini, W. Zhang, J. M. Ball, A. R. S. Kandada, H. J. Snaith and A. Petrozza, *Energy Environ. Sci.*, 2016, **9**, 3472–3481.

This journal is © The Royal Society of Chemistry 2017